COORDINATED ANALYSIS OF AN ION IRRADIATED CARBONACEOUS CHONDRITE SUGGESTS COMPLEX SPACE WEATHERING EFFECTS. D. L. Laczniak[1], M. S. Thompson[1], C. A. Dukes[2], R. V. Morris[3], S. J. Clemett[4], L. P. Keller[3], and R. Christoffersen[4]. Earth, Atmospheric, and Planetary Sciences Department, Purdue University, West Lafayette, IN, 47907 (dlacznia@purdue.edu), [2]Laboratory for Atomic and Surface Physics, University of Virginia, Charlottesville, VA, 22904, [3]ARES, NASA Johnson Space Center, Houston, TX 77058, [4]Jacobs, NASA Johnson Space Center, Mail Code XI3, Houston, TX 77058.

Introduction: Surfaces of airless planetary bodies are exposed to micrometeorite bombardment and solar wind irradiation which alter the microstructural, compositional, and optical properties of regoliths over time. These processes are collectively known as space weathering, and they complicate the interpretation of remote sensing data and the subsequent characterization of airless surfaces [1]. Within the next 5 years, NASA's OSIRIS-REx and JAXA's Hayabusa2 missions will return samples from C-type asteroids Bennu and Ryugu, respectively [2,3]. Compared to the Moon and S-type asteroids, our understanding of the space weathering of C-complex asteroids is limited [1]. In order to maximize scientific return from remote sensing data and to prepare for the analysis of returned samples from these missions, we must better understand the effects of space weathering on hydrated, organic-rich materials. We can do so by simulating these processes in the laboratory. In this study, we simulate solar wind exposure through ion irradiation of the CM2 carbonaceous chondrite Murchison—a suitable analog for C-complex asteroids [4]. Here, we present coordinated analyses of a sample before and after ion irradiation.

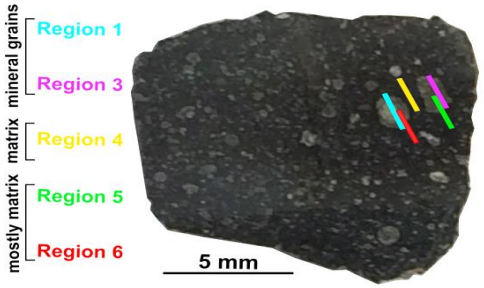

Figure 1: *Image showing matrix and mineral locations of XPS analyses irradiated with 4 keV He.*

Methods: We irradiated two discrete 6x6 mm^2 regions of a dry-cut Murchison chip under ultra-high vacuum. The first region was bombarded with 2 keV H^{2+} ions at a flux of $1.1x10^{13}$ ions/cm^2/s for a total fluence of $8.1x10^{17}$ ions/cm^2. The second area was bombarded with 4 keV He^+ ions at the same flux to a total fluence of $1.1x10^{18}$ ions/cm^2. We obtained surface compositional information from a PHI Versaprobe III Imaging X-ray Photoelectron Spectrometer (XPS) with a monochromatic, scanning X-ray source ($Al_{K\alpha}$: 1486.7 eV) and hemispherical electron-energy analyzer under ultra-high vacuum. Survey (wide scan) and detailed (narrow scan) spectra were taken at five different locations before and after irradiation: two from chondrule-bearing regions and three from the matrix (Fig. 1). To evaluate optical modifications, we collected visible to near infrared (VNIR; 0.35 – 2.50 µm) reflectance spectra from the pre- and post-irradiated samples using a fiber-optic ASD FieldSpec 3 Spectrometer (Malvern Panalytical) under ambient laboratory conditions. We investigated changes in organic functional group chemistry using the 118 nm photoionization spectral map acquired by the µL^{2}MS instrument at Johnson Space Center.

Surface Chemistry Results: XPS spectra before and after He^+ irradiation demonstrate consistency in Murchison's surface chemistry and oxidation state (Fig. 2). Carbon peaks are significantly lowered after He^+ irradiation, suggesting the destruction and removal of surface organic species. All other elements exhibit a commensurate increase in peak intensity [5].

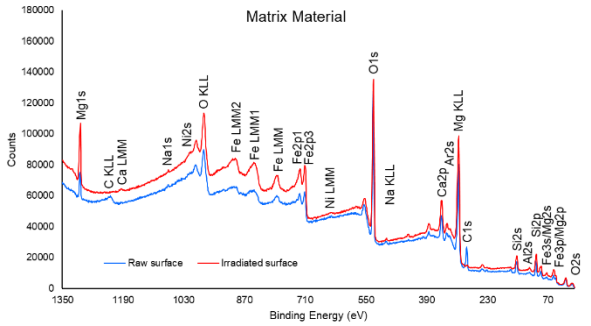

Figure 2: *Matrix survey XPS spectra before (solid) and after (dashed) He^+ irradiation. Labels correspond to element-specific photoelectron (e.g., Mg1s) and Auger transition (e.g., Mg KLL) peaks.*

Reflectance Spectroscopy Results: He^+ ion irradiation yields darkening (decrease in reflectance) shortwards and brightening (increase in reflectance) longwards of the 0.7 µm wavelength. Reddening of the reflectance spectrum also occurs in the He^+ irradiated sample (Fig. 3a). He^+ irradiated samples in [6] possess similar reddening and brightening trends. In contrast, the H^{2+} irradiated sample is similar in brightness to the unweathered surface. Both irradiated spectra show weakened ~1.0 µm (olivine or Fe^{2+} phyllosilicates), ~0.7 µm (Fe^{2+}-Fe^{3+} phyllosilicates), and ~1.94 µm (water) absorption bands (Fig. 3b), with He^+ inducing a more drastic change [7]. He^+ irradiation also slightly strengthens absorptions at ~0.44, 0.47, and 0.50 µm bands, of which the latter two correspond to Fe-oxides.

Organics Results: Of the 2-4% carbon abundance in CM chondrites, the majority of it occurs as organic

material and in the form of refractory complex hydrocarbons [8]. He^+ irradiation reduces the overall organic abundance by ~30-40% (Fig. 4). Concentrations of aromatic species remain relatively unchanged after irradiation, suggesting aromatics may be more resistant to irradiation-driven chemical and structural modifications compared to other organics. Subsequent mapping with 266 nm photoionization will highlight the chemistry and evolution of these aromatics.

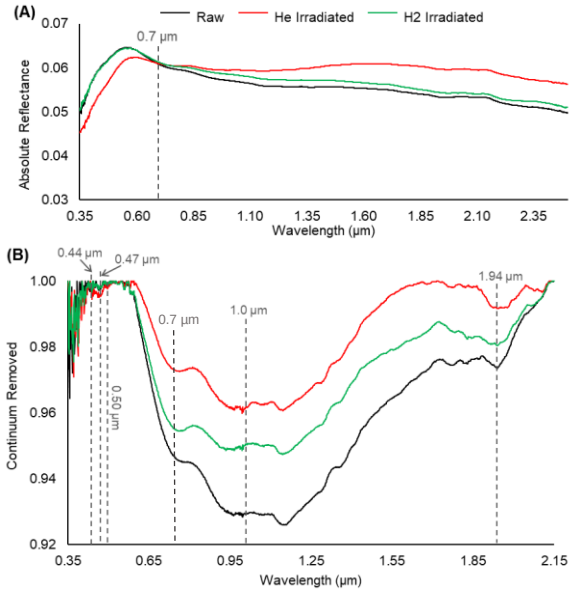

Figure 3: *(A) Absolute reflectance and (B) continuum removed reflectance of unirradiated (black), He^+ irradiated (red), and H^{2+} irradiated (green) Murchison samples.*

Implications for Space Weathering on Primitive Bodies: Ion irradiation of carbonaceous material yields complex spectral results. XPS data suggest minimal change in surface chemistry beyond the destruction of organic carbon. However, reflectance data indicates a more involved mineralogic alteration history. The irradiation-induced attenuation of the 0.7 and 1.0 µm bands reflects the breakdown of matrix phyllosilicates and possibly olivine, the partial reduction of iron from Fe^{3+} to Fe^{2+}, and/or minor production of nanophase particles [9]. The strengthening of bands near 0.47 and 0.50 µm may reflect the presence of Fe^{3+} bearing oxides (e.g., magnetite). This spectral signature may reflect nanophase oxide formation, which can occur in reducing environments in the presence of OH^-. In this experiment, such a process may be further supported by the weakening OH/H_2O band at 1.94 µm which would provide volatile phases necessary for oxide formation via loss of OH^- from phyllosilicates during irradiation. Similar trends were observed in pulsed-laser irradiation experiments conducted on Murchison chips [10].

Although irradiated surfaces lack a prominent red slope, they do redden compared to the unweathered Murchison sample. This could suggest the formation of nanophase metallic iron or sulfides in addition to nanophase oxides e.g., [1]. In contrast, the mechanism behind spectral brightening is uncertain. Creation and successive destruction of nanoparticles [8], organic chemical and/or structural changes, or increased surface roughness from irradiation are all possible causes [11]. The decrease in nearly all organic species (except aromatics) suggests He^+ irradiation destroys and volatilizes them. When these results are compared to organic analyses of pulsed-laser irradiation experiments in [8], He^+ irradiation appears to destroy a variety of organic species while pulsed-laser irradiation breaks down complex refractory hydrocarbons, leading to an increase in organic free species abundance. Future chemical and microstructural TEM analyses will help us correlate nanoscale features to the complicated spectral effects mentioned here.

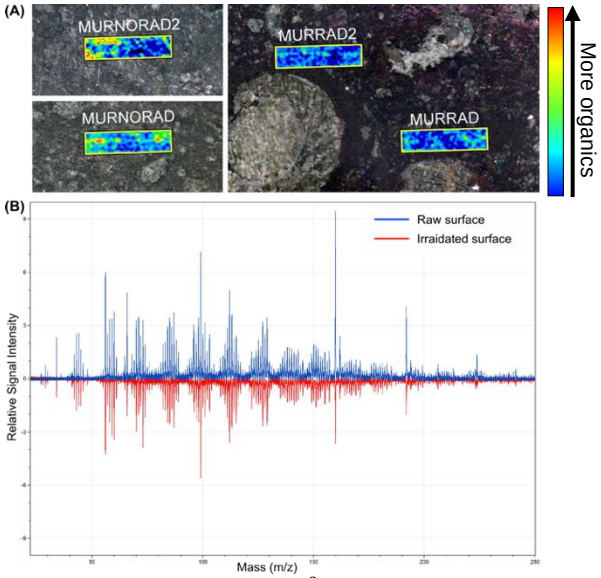

Figure 4: *Comparison of µL²MS data from the He^+ irradiated rock chip using 118 nm photoionization. (A) Organic chemical maps showing the sum of organic species in unirradiated (MURAD1&2) and irradiated (MUNORAD1&2) regions . (B) Spectral comparison of the sums of the two unirradiated (blue) and two irradiated (red) surfaces seen in (A).*

References: [1] Pieters, C. and S. Noble (2016), *JGR*, *121*(10), 1865-1884. [2] Lauretta, D. *et al.* (2015), *Meteorit. Planet. Sci.*, *50*, 834-849. [3] Yoshikawa, M. *et al.* (2015), IAU Gen. Assembly 22, 54481. [4] Clark, B. *et al.* (2011), *Icarus*, *216*, 462 – 475. [5] Loeffler, M. *et al.* (2009), *JGR*, *114*(E3). [6] Lantz, C. *et al.* (2015), *A&A*, *557*, A41. [7] Cloutis E. A. *et al.* (2012), *Icarus*, *220*, 586-617. [8] Matsuoka M. *et al.* (2017), *Icarus*, *254*, 135-143. [9] Keller, L. P. et al. (2015), LPSC XLVI, Abstract 1913. [10] Thompson, M. S., *et al.* (2018), *LPSC XLIX*, Abstract 2408. [11] Moroz, L. *et al.* (2004), *Icarus*, *170*, 214-228.